REVIEW ARTICLE

Initial Steps to Tracer Kinetic Modeling and MBF Quantification

Ran Klein, PhD[1), 2)]

Received: January 30, 2018/Revised manuscript received: March 8, 2018/Accepted: March 26, 2018
J-STAGE Advance published: July 27, 2018

Abstract

Kinetic modeling is gaining clinical relevance with wider adoption of myocardial blood flow quantification with PET. This work introduces the reader to the basic concepts of dynamic imaging, the one-tissue kinetic model, and tracer extraction correction. Key tracer specific nuances of kinetic modeling are highlighted. Finally, possible pitfalls which must be considered for accurate myocardial blood flow quantification are discussed.
Keywords: Dynamic PET, Kinetic modeling, Myocardial blood flow, Quantification
Ann Nucl Cardiol 2018; 4 (1): 68−73

One of the key advantages of nuclear imaging, particularly positron emission tomography (PET) imaging, is the quantitative nature of the images. Beyond the ability to semi-quantify uptake using standard uptake values with static PET, dynamic PET can measure radiopharmaceutical (tracer) concentrations across the imaging field of view as the tracer distributes and biochemically interacts within the living subject. These dynamic image sequences can be analyzed to derive rates of interaction using a model of the tracer kinetics (1).

Quantification of physiology using dynamic PET imaging has been successfully applied in many research applications (1, 2); however, clinically it is rarely applied due to extra imaging time, the need for image analysis and a lack of clear clinical justification. One exception is the growing application of dynamic PET for myocardial blood flow quantification (MBF) (3). MBF quantification has matured with regulator-approved image analysis software now commercially available. Thus, clinical applications have become a reality (4), but not without subtleties that could trip up the inexperienced.

This article aims to initiate the reader into the field of kinetic modeling within the context of MBF quantification, and to highlight common pitfalls that may be encountered during implementation and routine use.

Tracer distribution process

Before one can describe a kinetic model, the physiologic process that it represents must first be understood by tracing its path. Myocardial blood flow imaging begins with intravenous administration of a suitable tracer into the blood. The tracer is transported through the venous system, the right chambers of the heart, the lungs and the left chambers of the heart before entering the arterial system and perfusing the body. In the case of the heart itself, tracer is routed through the coronary arteries towards the capillary bed where the tracer may be extracted by the tissue. The amount of tracer in the blood that is made available to the tissue of interest is proportional to the blood flow to that tissue.

Removal of the tracer out of the blood and into the tissue is referred to as wash-in or uptake. Outside of the blood, the tracer passes through interstitial space and may then continue into the heart muscle cells (i. e. myocytes) where it may interact further. Once taken up, a tracer may be retained indefinitely (i.e. is trapped) in the extra-vascular space or it may gradually wash out over time. Consideration of the washout rate is important for accurate modeling and may also contain useful information incremental to flow.

For blood flow quantification we are primarily interested in the rate at which the tracer is taken up into the extra-vascular region and how quickly it washes out back into the blood

doi: 10.17996/anc. 18-00052

1) Ran Klein
The Ottawa Hospital, Department of Nuclear Medicine, Ottawa, Canada
E-mail: rklein@toh.ca

2) Ran Klein
Division of Nuclear Medicine, Department of Medicine, University of Ottawa, Ottawa, Canada

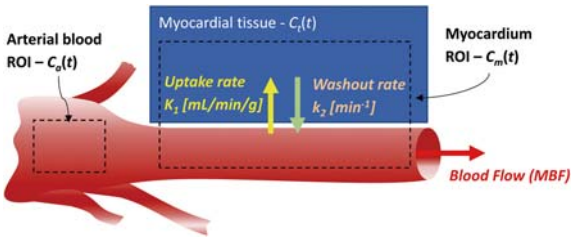

Fig. 1 One-tissue compartment model consisting of blood (red) perfusing myocardial tissue (blue) and tracer exchange between them (K_1 and k_2). Regions of interest (ROI) can be used to sample tracer time-activity concentrations curves $C_a(t)$ and $C_m(t)$ from the dynamic image sequence when placed on the larger arteries (e.g. left chambers of the heart, aorta) and myocardium respectively.

(uptake and washout rates-mathematically referred to as K_1 and k_2 respectively and illustrated in Fig. 1). Uptake rate is the product of blood flow and the first-pass extraction fraction; the fraction of tracer in the blood that is extracted by the tissue without recirculation of the blood to the tissue. Uptake may be limited by either flow or extraction fraction.

Ideally the uptake rate of the tracer is proportional (or even equal) to blood flow with high (approaching 1.0) and constant extraction fraction independently of the blood flow, as is the case with ^{15}O-water (see Fig. 2). However, water washes out of the myocardium just as freely, and therefore ^{15}O-water PET does not produce uptake images that are useful for traditional myocardial perfusion image interpretation. ^{18}F-Flurpiridaz also exhibits almost complete extraction, but is retained in the myocardium (as it binds to the mitochondria in the myocytes) resulting in superb perfusion images (5). In both these cases uptake is limited by flow and therefor MBF is (nearly) equal to uptake rate.

Other flow tracers such as ^{82}Rb-chloride and ^{13}N-ammonia are actively transported into the myocardium, which may limit their rate of uptake. Due to flow dependent variations in capillary surface area, blood pressure and blood velocity, these extraction rates may also be MBF dependent, resulting in a non-linear, diminishing extraction fraction with increasing MBF. Flow dependent extraction curves, such as shown in Fig. 2 (6-10) are typically derived empirically and may be used to relate uptake rates to MBF. Because extraction fraction decreases with flow (Fig. 2), the amount of required extraction correction increases correspondingly, which has the disadvantage of also amplifying noise in K_1 measurements (11, 12).

The above description relates the transfer of tracer between blood and a single tissue compartment, and the rates of transfer may be derived from changes in tissue and blood tracer concentration from time of tracer injection until uptake in the myocardium (13).

Dynamic imaging

To visualize the tracer distribution process, image acquisition must begin before tracer entry into the arterial system and continue until tracer distribution, uptake by the tissue and preliminary washout. For MBF quantification, imaging duration is typically on the order of 4 to 10 minutes. Short-lived tracers, such as ^{82}Rb and ^{15}O-water do not warrant imaging beyond ～6 minutes as little activity remains for imaging and uptake is usually completed by 3 minutes (14). Long dynamic image sequences (e.g. >8 minutes) may be warranted to observe slower physiologic processes which are obscured in earlier times, but may also require a correspondingly more complicated kinetic model than that discussed herein (15).

During image reconstruction, pre-determined time-frame intervals must be specified to generate a dynamic image sequence. Frames should be sufficiently short to accurately capture fast dynamics associated with first pass of the tracer and long enough to achieve a high number of detection events to generate sufficient image quality. Typically, dynamic imaging begins with a series of short time-frames (e.g. 5-10 second intervals for the first 90-180 seconds) and is followed by a series of longer time-frames (e.g. 30-120 seconds) for the remainder of the scan where dynamics are slow and less activity is present (16).

Tracer concentration sampling

Tracer concentrations may be derived from the dynamic image sequence by different methods, but the simplest and most common approach is to define one region of interest (ROI) overlaying a large arterial body (e.g. left ventricle, left atrium and/or aortic root) and multiple ROIs for regions of the myocardium. Sampling the activity concentrations in the ROIs over the dynamic image sequence produces corresponding arterial blood (17) and myocardium time-activity curves (TACs), labelled as $C_a(t)$ and $C_m(t)$ respectively in Fig. 1. TACs consist of a finite number of time-frames that approximate continuous functions.

TACs are typically represented in image units (usually Bq/mL), but because kinetic modelling relates input and output functions, the TAC units are not important in this context as long as both TACs are on a common scale. Each time-frame image must be appropriately scaled to correct for radioactive decay between time-frames so that the resulting TACs correspond to tracer concentrations due to distribution changes alone. Decay corrections are typically applied during image reconstruction, but can also be performed post-reconstruction.

Kinetic modeling

While models of varying complexity have been developed for different tracers and applications, the physiologic process for MBF tracers as described above can be adequately

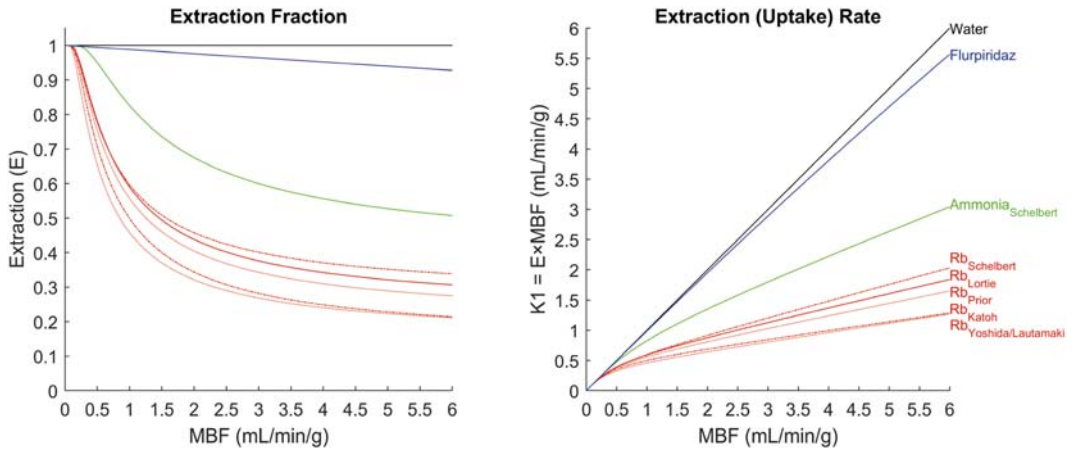

Fig. 2 Myocardial Blood Flow (MBF) dependent extraction fraction functions (left) and corresponding uptake rates (right) for common PET tracers.

modeled with a one-tissue compartment model of transfer between arterial blood, $C_a(t)$, and the tissue compartment, $C_t(t)$ as illustrated in Fig. 1.

The rate of change in tissue concentration at any given time, $dC_t(t) / dt$, is proportional to the amount of tracer in the arterial blood ($C_a(t)$), with the proportion representing the rate of uptake (K_1) in units of inverse time (e.g. min^{-1}). Likewise, the change in tissue concentration associated with tracer washout depends on the amount of tracer in the tissue compartment at a given time ($C_t(t)$) and the washout rate (k_2 [min^{-1}]). The units of K_1 are typically converted to a more convenient notation by accounting for the average density of tissue ($\rho \approx 1.04$ g/mL), and therefore K_1 is represented in units of mL/min/g, which is read as mL per minute of blood flow, per gram of tissue.

The change in tissue concentration, $dC_t(t)$, over a short time interval (dt [min]) may be written mathematically as shown in Equation 1 and can be converted to a more convenient convolution (symbolized as ⊗) form as shown in equation 2. Using assumed K_1 and K_2 parameters and measurements of changing arterial blood tracer concentrations from the start of imaging to time, t, the convolution form models the net accumulation of the tracer in the tissue over this time interval.

$$\frac{dC_t(t)}{dt} = K_1 \cdot \rho \cdot C_a(t) - k_2 \cdot C_t(t) \quad (1)$$

$$C_t(t) = K_1 \cdot \rho \cdot e^{-k_2 t} \otimes C_a(t) \quad (2)$$

Tissue partial volume modeling

Sampling of the myocardial tissue, $C_t(t)$, alone is impractical due to the presence of blood perfusing the tissue. The myocardium TAC, $C_m(t)$, also contains spillover blood signal from neighboring blood regions such as the left ventricle cavity, due to the limited spatial resolution of PET (6-12 mm) which is exacerbated by the presence cardiac motion. Therefore, $C_m(t)$ typically contains 20-40% arterial blood signal, $C_a(t)$, which must be accounted for (14). One common approach to correct for blood spillover is to include blood and tissue volume fractions (P_a and P_t respectively) in the model estimating the myocardial TAC, $\tilde{C}_m(t)$, using Equation 3.

$$\begin{aligned}\tilde{C}_m(t) &= P_t \cdot C_t(t) + P_a \cdot C_a(t) \\ &= \boldsymbol{P_t} \cdot \boldsymbol{K_1} \cdot \rho \cdot e^{-k_2 t} \otimes C_a(t) + Pa \cdot Ca(t)\end{aligned} \quad (3)$$

Since neither parameter P_t or K_1 are known, there is no unique solution to equation 3, requiring an additional assumption. Sometimes referred to as the Hutchin method (18, 19), equation 4 overcomes this problem by assuming that the arterial blood TAC, $C_a(t)$, is free of partial volume effects and that the myocardium TAC, $C_m(t)$, is comprised of arterial blood and myocardial tissue alone, without contributions from other signals, which is expressed as:

$$P_t + P_a = 1 \quad (4)$$

Thus, by combining Equations 3 and 4, the final form of the 1-tissue compartment model is obtained:

$$\tilde{C}_m(t) = (1 - P_a) \cdot K_1 \cdot \rho \cdot e^{-k_2 t} \otimes C_a(t) + P_a \cdot C_a(t) \quad (5)$$

Determining the kinetic-model parameters

Equation 5 is a complete model, relating the image derived arterial blood and myocardial TACs, $C_a(t)$ and $C_m(t)$respectively, and it has three unknown free parameters that need to be resolved (P_a, K_1 and k_2). To determine these parameters, $C_a(t)$ may be substituted into the equation and $\tilde{C}_m(t)$ may be calculated. The free parameters are adjusted using a fitting algorithm that minimizes a penalty function for the error between the modelled and image derived myocardial TACs, $\tilde{C}_m[i]$ and $C_m[i]$ respectively, where i denotes the time-frame number from the n time-frames in the dynamic image sequence. This process is also referred to as model optimization. To improve optimization performance, more

emphasis may be put on reducing error at certain image time-frames using an error weighting function, $W[i]$ (e. g. proportional to frame length). An example error penalty function is the sum squares:

$$E=\sum_{i=1}^{n} W[i]\cdot(\tilde{C}_m[i]-C_m[i])^2 \quad (6)$$

Relationship between TAC phases and model parameters

Simulated image sampled blood and myocardium TACs, $C_a(t)$ and $C_m(t)$ respectively, and fitted kinetic model are illustrated in Fig. 3 to demonstrate the relationship between model curve characteristics and model parameters. The fitted model myocardium TAC, $\tilde{C}_m(t)$, minimizes the error with the image-derived TAC, $C_m(t)$. The myocardium TAC is a linear combination of the blood and tissue TACs controlled by a single parameter, P_a. Fitting of P_a is primarily driven by the magnitudes of the myocardium curve in the early time-frames relative to the magnitude of the blood peak. The height of the tissue compartment TAC, $C_t(t)$, depends on the magnitude of K_1 and the integral of the blood TAC, and on P_a. The rate at which the tissue TAC decreases after the blood peak is moderated by k_2 and is dependent on the rate of exponential decrease of the myocardium TAC in the late time-frames, when little blood activity is present. Nevertheless, all three parameters are adjusted together to reduce the overall error penalty.

Extraction correction

Uptake values are converted to MBF using an extraction correction. Extraction functions, $E(MBF)$, are typically derived under varying flow conditions using reference MBF measurements (e.g. microspheres or another established MBF imaging method) and can then be applied to correct K_1 to estimate MBF:

$$MBF=K_1/E(MBF) \quad (7)$$

Since both sides of equation 7 are dependent on MBF the equation cannot be analytically solved; a look-up table of extraction correction factors may be precomputed as a technical workaround.

Discussion

This article is intended as a brief introduction to kinetic modeling and MBF quantification. MBF quantification often uses the simplest of the kinetic models－the one-tissue compartment model－making it a relatively accessible starting point into the foyer of kinetic modelling. Perhaps more impactfully, MBF is the most common application of kinetic modelling in nuclear cardiology and is growing in popularity. As MBF moves from the research laboratory into common clinical use, there is a need to educate a broader audience on its workings and pitfalls to achieve optimal quality. Several points to consider:

Linear imaging response

For accurate kinetic modeling, TACs must be proportional to tracer concentrations in the tissues of interest. Several corrections are implemented in PET to achieve a linear response over a wide range of activity concentrations, but limitations in count-rate capabilities remain an important point of consideration in imaging protocol design－more so with dynamic imaging than with post-uptake static imaging. As the tracer distributes from first-pass blood pool to the body tissues, not only does its concentration dramatically drop, so does the proportion of administered tracer that is in the camera field of view. Furthermore, with short-lived tracers such as ^{82}Rb, image acquisition time can span several radioactive half-lives. Thus, the image acquisition system is required to remain linear over several orders of magnitude of activity encountered in a single scan (20).

In combined cardiac imaging protocols where there is interest in producing both dynamic PET in addition to static and gated uptake images, one must adjust tracer administration to achieve both high-count uptake images while avoiding camera saturation in early, blood pool images (11, 20, 21). High-end systems utilizing LYSO crystals can accommodate higher count-rates and are therefore better suited to this task. Nevertheless, accurate MBF quantification has been demonstrated on lower count-rate capable BGO cameras using tailored doses and remains of interest due to lower costs (21).

Patient motion

An important assumption for TAC sampling is that corresponding ROIs are consistent with a specific anatomical region throughout the dynamic image sequence. This assumption may be violated in the presence of motion, such as gross patient motion or organ creep (e.g. organ motion within the patient). Ideally, these motions should be avoided or corrected, but this is not always possible and quality assurance should therefore exclude cases in which motion compromises kinetic model accuracy (11, 22). Cardiac motion, which is reciprocal and has a shorter period than typical frame lengths, produces a partial volume effect that is partially accounted for in equations 3-5. Respiratory motion, while also reciprocal, has periodicity that is on the same order as short time-frames and can produce large heart motion that could affect MBF accuracy. Motion between PET and attenuation correction maps can further compound errors by producing local image artifacts, especially at the boundary between heart and lung (23). Substantial research is currently devoted to motion correction, but quality assurance is paramount for accurate interpretation of MBF data.

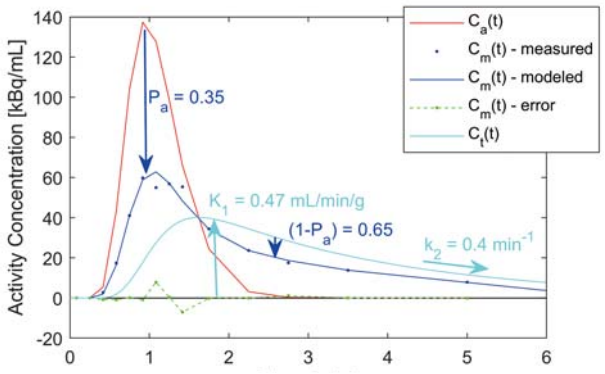

Fig. 3 Example image derived blood (red) and myocardium (blue dots) time-activity curves. A fitted kinetic model produced a myocardium time-activity curve (blue line) consist of a portion (P_a) blood and (1-P_a) modelled tissue response (cyan) as characterized by uptake and washout rates (K_1 and k_2, respectively). The error (green) between image derived and modeled myocardial curves is minimized for kinetic model parameter optimization.

Residual blood activity

In practice, blood TACs rarely decrease to absolute zero after tracer uptake (as demonstrated in Fig. 3), manifested by residual blood activity at late phases of the acquisition. Residual blood activity may be real due to tracer binding to blood components such as red blood cells, tracer impurities, or the accumulation of tracer metabolites in the blood. Residual blood activity may also be due to "contamination" from signal of neighboring tissues (e.g. myocardium) due to limited image spatial resolution (i.e. spillover effects), especially in small hearts. Uncorrected residual blood activity artifacts will result in overestimation of k_2. Image decomposition and dual spillover correction methods have been proposed as a solution to spillover effects, producing more reproducible results (10, 24-27).

Metabolite corrections

Some tracers may be metabolized in-vivo, producing radio-labelled metabolites. Since images do not distinguish between the tracer and its radio-labelled metabolites, these must be accounted for in the kinetic analysis. ^{13}N-ammonia and ^{11}C-acetate are two such examples in which the accumulation of metabolites in the blood can be corrected for using empirically determined functions (28, 29). Since metabolism may be variable between populations, population specific metabolite corrections may be warranted.

Extraction correction as a calibration function

When required, extraction correction functions typically use a modified Renkin-Crone model (30, 31), which models flow dependent tracer permeability and surface area of the compartment interface. In practice, experiments relate image-derived K_1 values to reference MBF measurements, producing a calibration function which compensates not only for tracer extraction, but also for any biases in K_1. This may partially explain variations in published extraction functions for similar tracers, as demonstrated for ^{82}Rb in Fig. 2. This subtle, but important, premise may warrant calibration between methods (e.g. instrumentation, imaging protocol, software) and perhaps even patient populations. Nevertheless, a growing body of evidence has already demonstrated standardization between software (32, 33), tracer administration (20), time-frame sampling (so long as they are sufficiently short) (11) and varying regions of interest (26, 27).

Conclusion

Kinetic modelling using dynamic PET has been researched, developed and applied since the early days of PET. It delivers non-invasive quantitative insight into the physiology of patients and research subjects and has thus been instrumental to basic science, pharmacology and clinical applications. Myocardial blood flow quantification using simple and robust kinetic modelling is being increasingly adopted for clinical use. While the basic principles are simple, many detailed considerations must be made for accurate and precise results. Thorough understanding of kinetic modeling is therefore vital not only to researchers, but also to those looking to apply myocardial blood flow clinically.

Acknowledgments

The author acknowledges the critical review and suggestions made by Jennifer Renaud from the University of Ottawa Heart Institute.

Sources of funding

None.

Conflicts of interest

Ran Klein is consultant with Jubilant DRAXimage and has received grant funding from industry partnership programs including GE Healthcare, Jubilant DRAXimage, Shelley Medical Solutions and Hermes Medical Solutions. Ran Klein receives revenues from rubidium generator technology licensed to Jubilant DRAXimage and revenue shares from the sale of FlowQuant®.

Reprint requests and correspondence:
Ran Klein, PhD
The Ottawa Hospital, P.O. Box 232, 1053 Carling Ave, Ottawa, ON, K1Y 4E9, Canada
E-mail: rklein@toh.ca

References

1. Watabe H, Ikoma Y, Kimura Y, et al. PET kinetic analysis－compartmental model. Ann Nucl Med 2006; 20: 583-8.
2. Schelbert HR. Positron emission tomography of the heart: methodology, findings in the normal and the diseased heart, and clinical applications. Phelps ME, PET, Springer, NewYork, 2004, 389-508. doi:10.1007/978-0-387-22529-6_6
3. Bengel FM. Leaving relativity behind: quantitative clinical perfusion imaging. J Am Coll Cardiol 2011; 58: 749-51.
4. Nesterov SV, Deshayes E, Sciagrà R, et al. Quantification of myocardial blood flow in absolute terms using ^{82}Rb PET imaging: the RUBY-10 study. JACC Cardiovasc Imaging 2014; 7: 1119-27.
5. Yalamanchili P, Wexler E, Hayes M, et al. Mechanism of uptake and retention of F-18 BMS-747158-02 in cardiomyocytes: a novel PET myocardial imaging agent. J Nucl Cardiol 2007; 14: 782-8.
6. Lortie M, Beanlands RS, Yoshinaga K, et al. Quantification of myocardial blood flow with 82Rb dynamic PET imaging. Eur J Nucl Med Mol Imaging 2007; 34: 1765-74.
7. Packard RR, Huang SC, Dahlbom M, et al. Absolute quantitation of myocardial blood flow in human subjects with or without myocardial ischemia using dynamic flurpiridaz F 18 PET. J Nucl Med 2014; 55: 1438-44.
8. Schelbert HR. Current status and prospects of new radionuclides and radiopharmaceuticals for cardiovascular nuclear medicine. Semin Nucl Med 1987; 17: 145-81.
9. Yoshida K, Mullani N, Gould KL. Coronary flow and flow reserve by PET simplified for clinical applications using rubidium-82 or nitrogen-13-ammonia. J Nucl Med 1996; 37: 1701-12.
10. Katoh C, Yoshinaga K, Klein R, et al. Quantification of regional myocardial blood flow estimation with three-dimensional dynamic rubidium-82 PET and modified spillover correction model. J Nucl Cardiol 2012; 19: 763-74.
11. Moody JB, Lee BC, Corbett JR, et al. Precision and accuracy of clinical quantification of myocardial blood flow by dynamic PET: A technical perspective. J Nucl Cardiol 2015; 22: 935-51.
12. Moody JB, Murthy VL, Lee BC, et al. Variance estimation for myocardial blood flow by dynamic PET. IEEE Trans Med Imaging 2015; 34: 2343-53.
13. Zierler K. A critique of compartmental analysis. Annu Rev Biophys Bioeng 1981; 10: 531-62.
14. Klein R, Beanlands RS, deKemp RA. Quantification of myocardial blood flow and flow reserve: Technical aspects. J Nucl Cardiol 2010; 17: 555-70.
15. Alessio AM, Bassingthwaighte JB, Glenny R. Validation of an axially distributed model for quantification of myocardial blood flow using ^{13}N-ammonia PET. J Nucl Cardiol 2013; 20: 64-75.
16. Lee BC, Moody JB, Weinberg RL, et al. Optimization of temporal sampling for 82 rubidium PET myocardial blood flow quantification. J Nucl Cardiol 2017; 24: 1517-29.
17. Weinberg IN, Huang SC, Hoffman EJ, et al. Validation of PET-acquired input functions for cardiac studies. J Nucl Med 1988; 29: 241-7.
18. Hutchins GD, Schwaiger M, Rosenspire KC, et al. Noninvasive quantification of regional blood flow in the human heart using N-13 ammonia and dynamic positron emission tomographic imaging. J Am Coll Cardiol 1990; 15: 1032-42.
19. Hutchins GD, Caraher JM, Raylman RR. A region of interest strategy for minimizing resolution distortions in quantitative myocardial PET studies. J Nucl Med 1992; 33: 1243-50.
20. Klein R, Ocneanu A, Renaud JM, et al. Consistent tracer administration profile improves test-retest repeatability of myocardial blood flow quantification with 82Rb dynamic PET imaging. J Nucl Cardiol 2016 [Epub ahead of print]. doi:10.1007/s12350-016-0698-6
21. Renaud JM, Yip K, Guimond J, et al. Characterization of 3-dimensional PET systems for accurate quantification of myocardial blood flow. J Nucl Med 2017; 58: 103-9.
22. Hunter CR, Klein R, Beanlands RS, et al. Patient motion effects on the quantification of regional myocardial blood flow with dynamic PET imaging. Med Phys 2016; 43: 1829.
23. Pourmoghaddas A, Vanderwerf K, Ruddy TD, et al. Scatter correction improves concordance in SPECT MPI with a dedicated cardiac SPECT solid-state camera. J Nucl Cardiol 2015; 22: 334-43.
24. El Fakhri G, Sitek A, Guérin B, et al. Quantitative dynamic cardiac 82Rb PET using generalized factor and compartment analyses. J Nucl Med 2005; 46: 1264-71.
25. Klein R, Beanlands RS, Wassenaar RW, et al. Kinetic model-based factor analysis of dynamic sequences for 82-rubidium cardiac positron emission tomography. Med Phys 2010; 37: 3995-4010.
26. Efseaff M. Test-Retest Repeatability of Myocardial Blood Flow Measurements using Rubidium-82 Positron Emission Tomography. Thesis for a degree, Ottawa-Carleton Institute for Physics, Department of Physics, Carleton University, 2012.
27. Ocneanu AF, deKemp RA, Renaud JM, et al. Optimally repeatable kinetic model variant for myocardial blood flow measurements with ^{82}Rb PET. Comput Math Methods Med 2017; 2017: 6810626.
28. Buck A, Wolpers HG, Hutchins GD, et al. Effect of carbon-11-acetate recirculation on estimates of myocardial oxygen consumption by PET. J Nucl Med 1991; 32: 1950-7.
29. van den Hoff J, Burchert W, Börner AR, et al. [1-^{11}C] Acetate as a quantitative perfusion tracer in myocardial PET. J Nucl Med 2001; 42: 1174-82.
30. Renkin EM. Transport of potassium-42 from blood to tissue in isolated mammalian skeletal muscles. Am J Physiol 1959; 197: 1205-10.
31. Crone C. The permeability of capillaries in various organs as determined by use of the ‘indicator diffusion’ method. Acta Physiol Scand 1963; 58: 292-305.
32. DeKemp RA, Declerck J, Klein R, et al. Multisoftware reproducibility study of stress and rest myocardial blood flow assessed with 3D dynamic PET/CT and a 1-tissue-compartment model of 82Rb kinetics. J Nucl Med 2013; 54: 571-7.
33. Dunet V, Klein R, Allenbach G, et al. Myocardial blood flow quantification by Rb-82 cardiac PET/CT: A detailed reproducibility study between two semi-automatic analysis programs. J Nucl Cardiol 2016; 23: 499-510.